Multiple structural transformations in Lennard-Jones clusters: Generic versus size-specific behavior

Vladimir A. Mandelshtam[a] and Pavel A. Frantsuzov
Chemistry Department, University of California at Irvine, Irvine, California 92697

(Received 1 March 2006; accepted 12 April 2006; published online 31 May 2006)

The size-temperature "phase diagram" for Lennard-Jones clusters LJ_n with sizes up to $n=147$ is constructed based on the analysis of the heat capacities and orientational bond order parameter distributions computed by the exchange Monte Carlo method. Two distinct types of "phase transitions" accompanied by peaks in the heat capacities are proven to be generic. Clusters with Mackay atom packing in the overlayer undergo a lower-temperature melting (or Mackay–anti-Mackay) transition that occurs within the overlayer. All clusters undergo a higher-temperature transition, which for the three-layer clusters is proven to be the 55-atom-core-melting transition. For the two-layer clusters, the core/overlayer subdivision is ambiguous, so the higher-temperature transition is better characterized as the breaking of the local icosahedral coordination symmetry. A pronounced size-specific behavior can typically be observed at low temperatures and often occurs in clusters with highly symmetric global minima. An example of such behavior is LJ_{135}, which undergoes a low-temperature solid-solid transition, besides the two generic transitions, i.e., the overlayer reconstruction and the core melting. © *2006 American Institute of Physics*.
[DOI: 10.1063/1.2202312]

I. INTRODUCTION

Atomic clusters exhibit very rich structural, thermodynamic, and dynamical properties that may vary with size in a nonmonotonous fashion. In particular, rare gas atomic clusters, often modeled using the Lennard-Jones (LJ) pair potential

$$U(r) = 4\epsilon[(\sigma/r)^{12} - (\sigma/r)^6], \tag{1}$$

have been very popular in the last several decades.

In the thermodynamic limit ($n \to \infty$) the properties of a monoatomic LJ system become relatively simple. This is because the only funnel of the potential energy surface that is thermodynamically stable below the melting transition is that corresponding to the global face-centered-cubic (fcc) energy minimum. Moreover, due to its translational invariance, the properties of a monoatomic bulk system are uniform in space and, under not very high pressures, are characterized by a simple phase diagram which only contains the solid, liquid, and gas phases. A complexity in bulk systems, such as a glassy behavior, may arise in binary mixtures. By contrast, finite even monoatomic systems, such as clusters, typically have multifunnel potential energy landscapes at low energies, which are responsible for their complex behavior.[1] An interesting question is how the cluster properties change with size when the thermodynamic limit is being approached. The answer to this question using accurate (all-atom) numerical simulations for the LJ case is hardly possible to obtain as even clusters with many thousands of atoms are still far from the thermodynamic limit.[2] While the latter must have the symmetry of a fcc lattice, the icosahedral symmetry is favored for finite sizes both energetically and entropically. Because for this size range the structure of the potential energy surface is sensitive to the cluster size, the question of which cluster properties are generic and which are size specific emerges naturally. The present paper tries to address this question for LJ_n clusters with sizes up to $n=147$.

The multifunnel nature of the potential energy surface of LJ clusters make their numerical simulations very challenging. The computer performance is gradually increasing in time: some of what was impossible several years ago, even using the most efficient algorithms, becomes possible today. The first converged result of the caloric curve for LJ_{38} was reported only in this millennium.[3,4] In the particular case of $n=38$ there exist two funnels at low energies representing octahedral (Oh) and icosahedral (ico) energy minima[5] leading to a pronounced size-specific behavior at low temperatures, which is especially difficult to simulate. The first numerical success[3,4] was due to both the use of the efficient exchange Monte Carlo (EMC) method[6,7] and the available computer power that was just sufficient to get the converged results. In a later paper[8] Frantz continued the numerical endeavor started in Refs. 3 and 4 now reporting the EMC calculations of heat capacities for LJ_n clusters up to $n=60$. He discovered that for some clusters, well below the evaporation temperature, the caloric curves $C_V(T)$ have two peaks. Although one is always tempted to attribute such peaks to some kind of phase transitions, the latter are not strictly defined for finite systems, possibly making such interpretations questionable. Furthermore, for the size range ($n \leqslant 60$) considered by Frantz one peak was typically much less pronounced than the other. Basing his arguments on the assumption that a

[a]Electronic mail: mandelsh@uci.edu

single thermally induced melting transition always takes place, the author did not give a clear interpretation of the double feature in the caloric curve behavior.

In a recent paper[9] (Paper I) we reported our preliminary results attempting to characterize the size-temperature "phase diagram" of LJ_n clusters, including sizes up to $n=147$, i.e., covering a much larger size range than what had been considered so far by other authors.

In Paper I we also observed two peaks in the $C_V(T)$ curves not only for the two-layer LJ_n clusters, but also for a wide range of three-layer LJ_n clusters. For the larger clusters both peaks turned out to be much more pronounced than for the size range ($n \leqslant 60$) considered by Frantz. Using mainly the continuity arguments, we suggested the following interpretation. The clusters with "magic numbers" of atoms ($n=13$, 55, and 147) form complete Mackay icosahedral structures and as such are most stable with respect to structural transformations. For most intermediate sizes the equilibrium low-temperature structure can roughly be represented as a Mackay icosahedral core with an incomplete overlayer.[10–13] The two major peaks observed in a large fraction of clusters correspond to two distinct structural transformations. The lower-temperature transformation occurs in clusters with sizes $31 \leqslant n < 55$ and $82 \leqslant n < 147$ (except $n=85$). Most of these clusters have Mackay icosahedral global minima with incomplete Mackay overlayers, which we further abbreviate as "ico(M)." The exceptions include sizes $n=38$, 98, and 102–104 corresponding to highly symmetric but nonicosahedral global minima. For each of these special cases, a finite temperature interval still exists in which Mackay icosahedral local minima, due to their higher entropies, appear thermodynamically more favorable than the nonicosahedral global minimum. For all the specified sizes (i.e., $31 \leqslant n < 55$, $82 \leqslant n < 147$, and $n \neq 85$), the anti-Mackay (or polyicosahedral) configurations, further abbreviated as "ico(aM)," are least energetically favorable. However, they have the highest entropy[14] and as such may become thermodynamically more favorable at sufficiently high temperatures and may lead to a peak in the heat capacity curve. Most of the two-layer clusters with $13 < n \leqslant 30$ and three-layer clusters with $55 < n \leqslant 81$ and $n=85$ have anti-Mackay global minima. The exceptions are LJ_{75-77} having decahedral (dec) global minima. The anti-Mackay clusters do not undergo the specified low-temperature structural transformation. Several global minima configurations that are representative of the two structural motifs, i.e., ico(M) and ico(aM), are depicted in Fig. 1. One can notice that the atom packing in an anti-Mackay overlayer is less compact than that in a Mackay overlayer. This suggests that considering them as isolated entities, the former has a more liquidlike character than the latter.

Although not based on converged calculations, evidences of surface melting in the LJ and other clusters were found and investigated previously.[15–19] References 17 and 18 explicitly attribute this transition for certain clusters to the Mackay-to-anti-Mackay (M→aM) type. The first quantitatively accurate description of the thermally induced M→aM structural transformation was given by Calvo and Doye[14] for the case of the LJ_{31} cluster, which displays two peaks in the $C_V(T)$ curve. They characterized the M→aM transition that occurs at $T \approx 0.027$ (using the reduced units ϵk_B^{-1}) as "solid-solid." The second and biggest peak at $T \approx 0.3$ was then associated with "the melting."

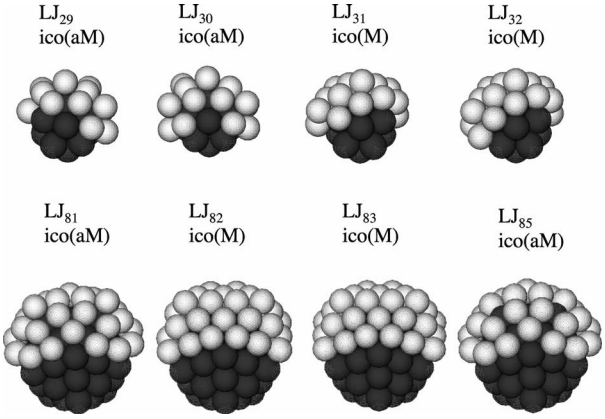

FIG. 1. Global minima configurations that are representative of the two typical structural motifs, i.e., the Mackay and anti-Mackay icosahedra. (The core atoms are shown in dark color.) The anti-Mackay overlayers are less compact and as such have a more liquidlike character.

Paper I suggests that the two transitions occurring in LJ_{31} also occur in all LJ_n clusters with $31 \leqslant n < 55$ and tries to justify it by the continuity argument. That is, the small peak in the $C_V(T)$ curve that first appears for $n=31$ persists for larger clusters while gradually shifting to higher temperatures and also becoming bigger in size (see the left panel of Fig. 2). The growth of the peak weight (which is directly related to the specific heat) is explained by the growing number of atoms in the overlayer that are involved in the transition, while the shift to higher temperatures is explained by the growth of the energy gap between the Mackay global minimum and the anti-Mackay local minima. One can also

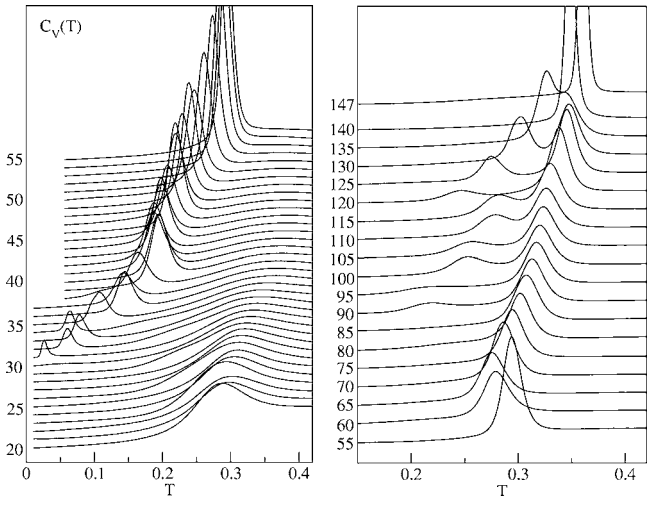

FIG. 2. Heat capacities $C_V(T)$ (per atom) for two- ($n=20-55$) and three-layer ($n=55-147$) LJ clusters. The curves are shifted along the y axis for a better visualization. The y labels indicate cluster sizes n. One can see the birth of the lower-temperature peak, which is due to the M→aM transition within the overlayer. It then increases in height and shifts to higher temperatures with increasing number of atoms in the overlayer. The higher-temperature peak is due to the melting of the cluster core. For the two-layer clusters, this peak broadens with increasing n and becomes less prominent, while for the three-layer clusters, it remains narrow and can be identified unambiguously untill the two peaks merge ($n \geqslant 140$).

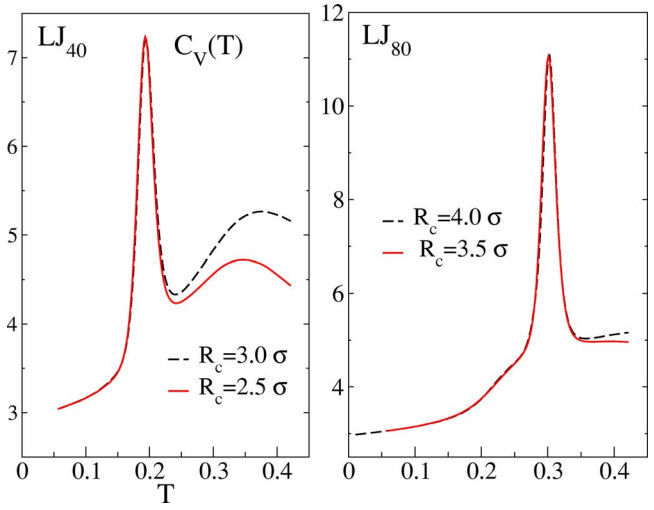

FIG. 3. Heat capacities $C_V(T)$ for two clusters using two different values of the constraining radius R_c. The sensitivity of $C_V(T)$ to R_c increases with temperature, which for the two-layer clusters may lead to an ambiguity in the location of the broad higher-temperature peak at $T\sim0.35$. LJ_{80} represents the three-layer clusters, for which the core-melting peak ($T\sim0.3$) is big and narrow, so it is unaffected by the change of R_c.

follow the higher-temperature peak with the increasing cluster size. Because this second peak becomes gradually broader and less pronounced, both its identification and interpretation are not easy without the continuity argument. Furthermore, as demonstrated in Fig. 3 for $n=40$ its shape is sensitive to the radius R_c of the constraining sphere used in the simulations. However, for the three-layer clusters for which LJ_{80} corresponds to a typical case (see Fig. 3), the higher-temperature peak is sufficiently big and sharp and as such can be identified unambiguously for all clusters. Paper I suggests that this higher-temperature peak is due to the melting of the cluster core, which for the $13<n<55$ size range resembles the global minimum of LJ_{13} and for $55<n<147$, the global minimum of LJ_{55}, both cores (LJ_{13} and LJ_{55}) being complete Mackay icosahedra. Perhaps because for LJ_{38} the peak at $T\approx0.35$ is too broad, this feature of the caloric curve is not even mentioned in Refs. 3 and 4 while the most pronounced peak at $T\approx0.15$ is associated with the melting, i.e., "the solid-liquid" transition of the cluster. According to our interpretation this peak corresponds to a M→aM transition. This implies the existence of an apparent inconsistency in the previously published studies in assigning qualitatively the same structural type, ico(aM), to either "solidlike" (for LJ_{31}) or "liquidlike" (for LJ_{38}). This issue becomes even more puzzling for clusters with anti-Mackay global minima. On the one hand, one usually assumes the system to be solid when it is at equilibrium at zero temperature. On the other hand, the structure of LJ_{30} at any temperature below $T\approx0.3$ including the $T=0$ point is similar to that of LJ_{31} above the M→aM transition, with the number of anti-Mackay isomers in both cases growing gradually with the increasing temperature. For LJ_{38} the number of thermodynamically stable isomers just above the M→aM transition is very large. Even though neither solid nor liquid assignment is strictly valid, perhaps a most consistent characterization of the anti-Mackay motif corresponds to a solidlike core with a liquidlike overlayer.

TABLE I. The cluster sizes n, the constraining radii R_c, and the typical numbers of MC steps per temperature used in the present EMC calculations for the four groups of clusters.

Group	Sizes n	R_c/σ	N_{MC}
A	10–40	2.5	1.5×10^9
B	20–57	3.0	2.0×10^9
C	50–80	3.5	5×10^9
C*	75–77	3.5	2.5×10^{10}
D*	80–147	4.0	5×10^{10}

In the present work we perform numerical simulations using both the more efficient adaptive EMC method and much longer random walks. The new results, albeit better converged, are not qualitatively different from those in Paper I. The second-order (Q_l) and the third-order (W_l) invariants[20] have been used in the past as symmetry markers for the structural analysis of clusters (see, e.g., Refs. 3 and 21). Here, in order to support our interpretations, as described above, we also use the orientational bond order parameters Q_4 and Q_6 for the analysis of cluster structures.

II. COMPUTATIONAL DETAILS

For each cluster an EMC calculation was carried out on a single Opteron processor and, depending on the cluster size, took from several days to several months of CPU time. In addition to the results reported in Paper I, in the present work the most significant effort was spent on performing new calculations for the size range $n\geqslant82$, for which the results in Paper I were not quite converged. For the special case of LJ_{75-77} clusters with nonicosahedral global minima, for which the results in Paper I were also nonconverged, converged results with their detailed analysis are reported in Ref. 22.

For all n we used a hard constraining sphere with four different radii for four different groups of clusters with overlapping size ranges (see Table I). To reduce the computational burden for large clusters we only considered sizes $n=90$, 95, 100, 105, 110, 115–120, 125, 130, 135, 140, and 147.

For all calculations the algorithm implementation was similar to that described in Ref. 3, except for the choice of the set of replica temperatures $T_1<T_2<\cdots<T_K$. Our original choice in Paper I for groups A, B, and C was made according to the simple recipe of Ref. 23 corresponding to a geometric sequence of $T_k=T_{\min}\lambda^k$. For a constant heat capacity such a temperature schedule would give uniform swap rates between adjacent replicas. The total number K of temperatures was varied from 20 to 40 depending on the cluster size and temperature range. For each n the latter was chosen according to the expected nontrivial behavior of the $C_V(T)$ curve, ranging from temperatures as small as $T_{\min}=0.01$ to $T_{\max}=0.42$, which is sufficiently large for the Metropolis random walk to sample the configuration space efficiently. The swaps of configurations between the random walks at adjacent temperatures were attempted every once in 100 MC steps per temperature, where one MC step corresponds to an attempt to move one of the atoms using the Metropolis

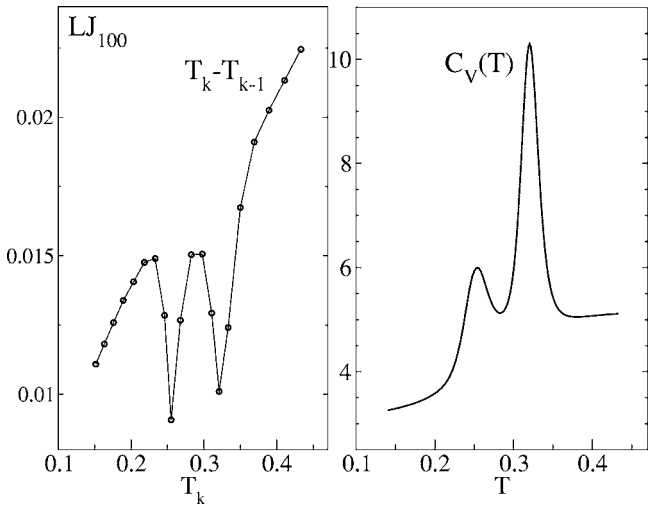

FIG. 4. The optimized temperature grid containing $K=21$ points T_k actually used in the present work for the LJ_{100} cluster. It was obtained self-consistently during the first 10^9 MC steps with the constraint that the mean exchange rate between replicas with adjacent temperatures T_k and T_{k-1} was 50%. The inverted plot of T_k-T_{k-1} vs T_k resembles the heat capacity $C_V(T)$, which is shown in the right panel for comparison. The latter was averaged over $N_{MC}=3.5\times10^{10}$ MC steps after $N_{equil}=1.5\times10^{10}$ equilibration steps.

scheme. In most cases the swap rates were about 50% or greater. However, at specific temperatures corresponding to large peaks in the heat capacity curves the swap rates were noticeably below 50%.

For the new calculations (groups C^* and D^*), in order to improve the convergence rates, we used self-adapted replica temperatures. The goal was to optimize the temperature schedule so that the mean exchange rate between replicas with adjacent temperatures T_k and T_{k+1} would be about 50% and remain approximately constant with k. To this end an optimal temperature schedule was chosen self-consistently following the procedure described by Hukushima and Nemoto.[7] During this self-consistent calculation T_1 was set equal to the lowest temperature of interest T_{min}, while the total number of replicas K was determined from the condition $T_K \geqslant T_{max}$. As an example in Fig. 4 we show the optimized grid actually used for the LJ_{100} cluster. It was obtained during the first 10^9 MC steps. Relative to the main calculation, the running time needed for the grid optimization is negligible, while the gain due to the accelerated convergence may be substantial. Moreover, since the grid optimization actually contributes to the equilibration process, no numerical effort is wasted. The optimal schedule is essentially geometric, except near the transition temperatures, where an accumulation is observed. Note though that the local minima in the optimized temperature schedule may accurately reproduce the transition temperatures only using a sufficiently long calculation.

Even though the EMC algorithm may seem to be a breakthrough in solving the problem of "broken ergodicity" at low temperatures, it may still encounter ergodicity problems for the reasons described below. Similar discussions of the convergence of the EMC method can be found in Refs. 24 and 25 for the particular case of LJ_{38} and in Ref. 22 for LJ_{75}. Configurations corresponding to the global or local minima that are thermodynamically favored at some low temperatures may belong to very narrow funnels of the potential energy landscapes and as such are extremely hard to find by a Monte Carlo search even in the EMC framework. Moreover, these funnels may be separated from the rest of the configuration space by large potential barriers which would also make it difficult for the replicas to either enter or exit such a funnel. In such cases the equilibration times using an arbitrary initial configuration may be very long. In order to improve on this difficulty, at least partially, we took the advantage of having the knowledge of the global minima[26] and used them as initial configurations for all the random walks. With this choice the equilibration times may still be very long if there is another funnel, which is thermodynamically favorable at some low temperatures, but also having the unfavorable properties specified above. This situation often occurs for systems with low-temperature structural transitions (i.e., typical for the LJ clusters) and rapidly worsens with the increasing cluster size. Unfortunately, we are not aware of any procedure to correctly incorporate the information on more than one funnel in the EMC calculation without having an *a priori* knowledge of the relative weights between different funnels contributing to the thermodynamic properties at various temperatures.

In order to make our results independent of the Lennard-Jones parameter ϵ we use the unitless variables for the temperature and energy

$$T = k_B T'/\epsilon, \quad E = E'/\epsilon, \tag{2}$$

where T' and E' define the original (nonreduced) quantities. If now $\langle E\rangle_T$ is the thermally averaged potential energy of the LJ_n cluster, the heat capacity is defined as

$$C_V(T) := \frac{1}{n}\frac{\partial}{\partial T}\left(\frac{3nT}{2} + \langle E\rangle_T\right)_V, \tag{3}$$

where we also included the kinetic energy contribution. Note that we use the partial (i.e., normalized by the cluster size n) heat capacity, which is more appropriate for analyzing it as a function of n. The heat capacities were computed using the standard fluctuation formula

$$C_V(T) = \frac{3}{2} + \frac{1}{nT^2}(\langle E^2\rangle_T - \langle E\rangle_T^2). \tag{4}$$

The canonical averages between the replica temperatures ($T_k < T < T_{k+1}$) were interpolated using the following expression

$$\langle A\rangle_T \approx \alpha_k(T)A_k(T) + [1-\alpha_k(T)]A_{k+1}(T), \tag{5}$$

where

$$\alpha_k(T) = \cos^2\left[\frac{\pi(T-T_k)}{2(T_{k+1}-T_k)}\right]$$

and

$$A_k(T) = \frac{1}{N_{MC}}\sum_{n=1}^{N_{MC}} \exp\left[\left(\frac{1}{T_k}-\frac{1}{T}\right)E(q_n^{(k)})\right]A(q_n^{(k)}). \tag{6}$$

Here $\{q_n^{(k)}\}$ $(n=1,\ldots,N_{MC})$ defines a Metropolis random walk generated at temperature T_k. As long as $\alpha_k(T)$ is a

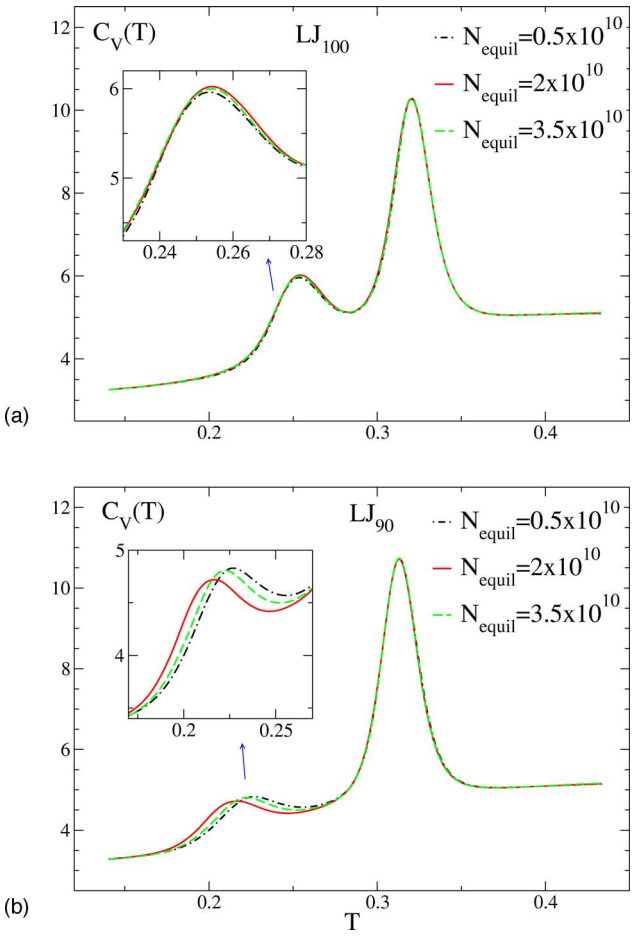

FIG. 5. Heat capacities for LJ_{100} and LJ_{90} clusters using different numbers of equilibration steps N_{equil} but the same number of accumulation steps $N_{MC}=1.5\times10^{10}$. LJ_{90} represents one of the worst cases, for which the convergence of the low-temperature peak may seem to be unsatisfactory.

smooth function with $\alpha_k(T_k)=1$ and $\alpha_k(T_{k+1})=0$, its choice is not important.

Note that, in principle, Eq. (6) alone gives an exact expression for $\langle A\rangle_T$ for any T and T_k in the $N_{MC}\to\infty$ limit. However, practically, it can be used only when the difference $T-T_k$ is not too large; otherwise its numerical convergence is very poor.

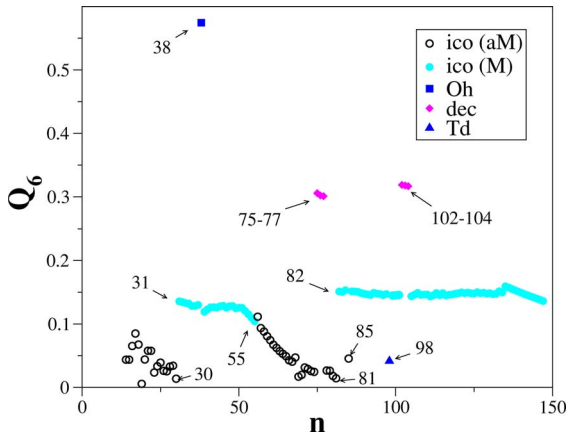

FIG. 6. Orientational bond order parameter Q_6 as a function of cluster size obtained from the global minima of LJ_n clusters. The following symmetry types are identified: Mackay icosahedral [ico(M)], anti-Mackay icosahedral [ico(aM)], truncated octahedral (Oh), decahedral (dec), and tetrahedral (Td).

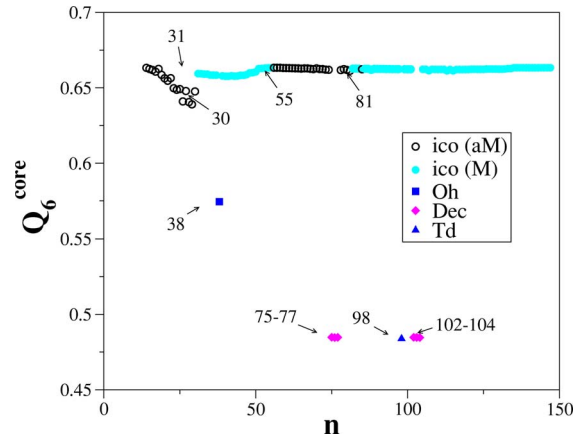

FIG. 7. Orientational bond order parameter Q_6^{core} evaluated over the core atoms of the global minima of the LJ_n clusters. Q_6^{core} is ambiguous for the nonicosahedral configurations. The deviations of Q_6^{core} from the value (0.663) corresponding to the complete icosahedra (LJ_{13} and LJ_{55}), especially for small clusters with an anti-Mackay overlayer, are due to the core distortion by the outer atoms.

In each EMC calculation the energy moments $\langle E\rangle_T$ and $\langle E^2\rangle_T$ were partially averaged and recorded after every $N_{MC}=5\times10^7$ MC steps per temperature. The convergence was then monitored by comparing results obtained from independent runs.

Alternatively, the caloric curve can be reconstructed from the distribution of potential energies gathered from all random walks using a multiple-histogram reweighting procedure.[27] We performed such a calculation for LJ_{75} in Ref. 22, but the heat capacities using this least-squares fitting procedure and the interpolating scheme turned out to give identical results. In the parallel tempering framework, including contributions from different replicas cannot improve statistical errors at any given temperature because, due to the frequent exchanges, all replicas are highly correlated. This made us believe that unless the microcanonical density of

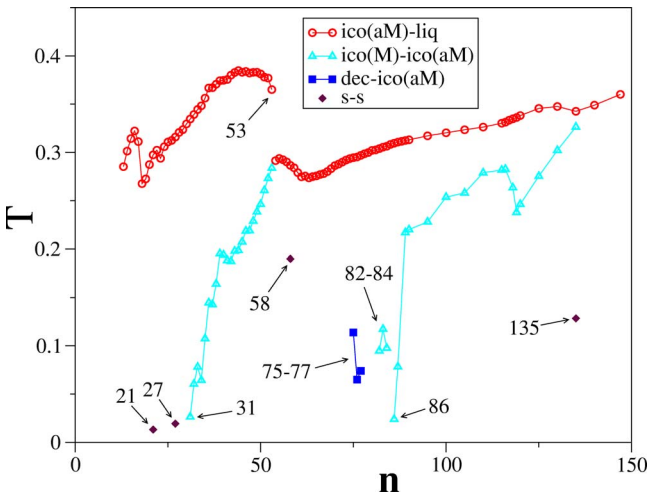

FIG. 8. Temperatures of the peak maxima of the $C_V(T)$ curves as a function of the cluster size n. The following structural transformations are identified: the Mackay-to-anti-Mackay [ico(M)-ico(aM)], core-melting [ico(aM)-liq], and decahedral-to-anti-Mackay [dec-ico(aM)] transitions. "s-s" define peaks accompanying transitions involving certain rearrangements of the overlayer atoms, but which we could not characterize in a generic manner.

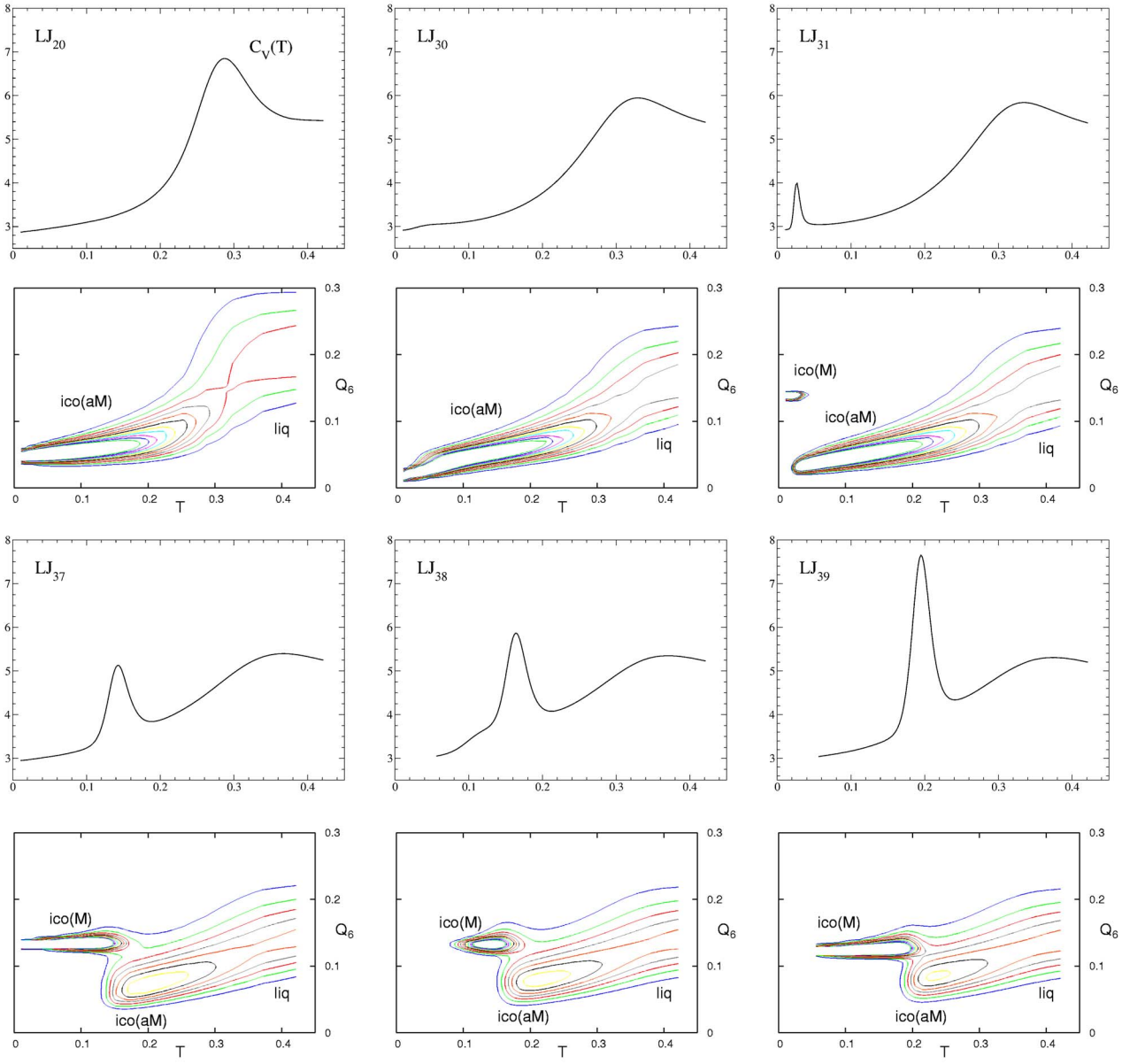

FIG. 9. The heat capacities $C_V(T)$ of selected two-layer LJ clusters. Also shown, under each heat capacity plot, is the contour plot of the corresponding distribution $\rho(Q_6,T)$ of the orientational bond order parameter Q_6. The contour levels were somewhat adjusted to best show the distinct features of the distributions. All clusters, except LJ_{38}, display the generic behavior depending on whether the global minimum has a Mackay or an anti-Mackay overlayer. An expansion of the $\rho(Q_6,T)$ plot for LJ_{38}, also showing the octahedral minimum, is given in Fig. 10.

states and related properties are of interest, for calculating canonical averages only, the multihistogram method may not be computationally advantageous.

We believe that our heat capacities for sets A, B, and C (C*) are converged within the widths of the curves, which was verified by comparing independent calculations. However, we note that, strictly speaking, such convergence tests cannot be valid, in particular, because we never used random initial conditions. Unfortunately, in the present work performing a more rigorous error analysis would be unfeasible as we already exhausted all the available computer resources. For set D*, the low-temperature peaks in the heat capacities are probably still not well converged for some sizes, for which, given the total length of the random walks, $n=5\times10^{10}$, we were not able to observe a satisfactory consistency when comparing independent calculations. Figure 5 shows two cases: LJ_{100}, for which the heat capacities seem well converged, and LJ_{90}, for which the position of the low-temperature peak still depends on the number of equilibration steps N_{equil}.

For the analysis of cluster structures we computed the thermal distributions $\rho(Q_4,T)$ and $\rho(Q_6,T)$ of the orientational bond order parameters Q_4 and Q_6 (Ref. 20) defined as

$$Q_l = \left(\frac{4\pi}{2l+1} \sum_{m=-l}^{m=l} |\bar{Q}_{lm}|^2 \right)^{1/2}, \tag{7}$$

with

$$\bar{Q}_{lm} = \frac{1}{N_b} \sum_{r_{ij}<r_b} Y_{lm}(\theta_{ij}, \phi_{ij}), \tag{8}$$

where $Y_{lm}(\theta, \phi)$ are the spherical harmonics and the sum is taken over some suitable set of "bonds" with $r_b = 1.392\sigma$. We considered two types of averages: (i) corresponding to the use of all near neighbors in the cluster and (ii) using only the bonds connecting the central atom with the atoms that belong to the cluster core. The corresponding value of the order parameter is then defined by Q_l^{core}. For clusters with $n < 55$ the cluster core is assumed to contain $n_{\text{core}} = 13$ atoms and for $55 \leqslant n \leqslant 147$, $n_{\text{core}} = 55$ atoms. For a general configuration it is not simple to identify a group of atoms which best fits the complete Mackay icosahedron. For the present case we adapted a procedure, which is a modified version of that described in Ref. 3. We found that using only the Q_4 order parameter, as in the latter work, to identify the cluster core is insufficient. Even though its use seems natural as it vanishes for a perfect icosahedron, for clusters with an incomplete overlayer the core is distorted giving a nonzero value of Q_4^{core} that may lead to a wrong assignment. To make the core identification more robust we also used the Q_6^{core} order parameter, which gives the value of about 0.663 for the global minima of both LJ_{13} and LJ_{55}. For each configuration analyzed the atom closest to the cluster center of mass is assumed to be the central atom of the core. Then $n_{\text{core}} - 1$ atoms closest to the central atom are selected, and the parameters Q_4^{core} and Q_6^{core} are evaluated. The procedure is then repeated nine more times by constructing the core around the next closest to the center of mass atom. Among all the computed pairs $(Q_4^{\text{core}}, Q_6^{\text{core}})$ the one minimizing the sum $(Q_4^{\text{core}})^2 + (Q_6^{\text{core}} - 0.663)^2$ is then assumed to represent the cluster core. Clearly, this procedure gives meaningful results only when the core can be identified in principle. Unfortunately, for two-layer clusters ($n < 55$) with an anti-Mackay overlayer the local icosahedral coordination of the LJ_{13} is typical, making the core/overlayer subdivision nonunique. The good news though is that this problem disappears for larger, three-layer clusters, for which the LJ_{55} core can generally be identified unambiguously.

RESULTS AND DISCUSSION

Figures 6 and 7 show the orientational bond order parameters Q_6 and Q_6^{core} obtained from the global minima of LJ_n (Ref. 26) as a function of n. (Here the choice for the order parameter Q_6 is motivated by its high sensitivity to the cluster symmetry, while we find Q_4 to be not as good to distinguish between certain symmetry types.) The diagram in Fig. 6 clearly distinguishes the two dominant (Mackay and anti-Mackay) structural types that are realized for all but several special cases ($n = 38$, 75–77, 98, and 102–104). At zero temperature the size-induced M→aM transitions occur at sizes 31→30 and 82→81. (Note though that LJ_{85} has an anti-Mackay overlayer.) Figure 7 demonstrates that for clusters with $n > 55$ the 55-atom-core configuration is quite stable, while for smaller clusters the 13-atom core may be significantly distorted by the presence of the overlayer atoms, especially in the case of the anti-Mackay overlayer.

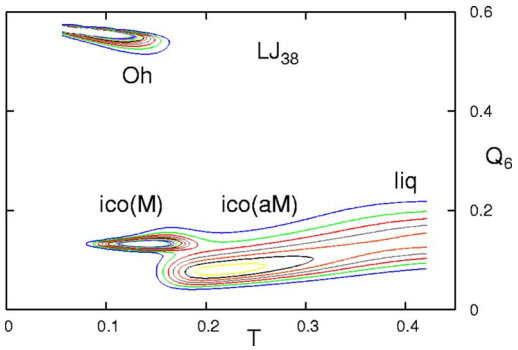

FIG. 10. The entire distribution $\rho(Q_6, T)$ for LJ_{38} showing all four different structural types including the octahedral global minimum configuration (Oh), which is thermodynamically favored at $T < 0.12$.

Heat capacities for selected clusters are shown in Fig. 2. For each n we estimated the temperatures at which the $C_V(T)$ curve has local maxima. The corresponding temperature-size diagram is shown in Fig. 8. For all cluster sizes considered $C_V(T)$ has at least one peak. For most clusters with a Mackay global minimum $C_V(T)$ has at least two peaks. Exceptions are LJ_{88} and LJ_{117}, for which the tail from the core-melting peak is relatively too large, resulting in the shoulder in $C_V(T)$ instead of a peak (see Fig. 11 below). Also for clusters with $n > 135$, i.e., close in size to the complete icosahedron, the two peaks merge. In these cases, the overlayer is most stable.

For the two-layer clusters, the higher-temperature peak gradually broadens with the increasing size. Moreover, as demonstrated in Fig. 3, the position of its maximum is quite sensitive to the value of the constraining radius: for R_c large enough the maximum may even disappear. Thus, the high-temperature transition for clusters with $n < 55$ can only be characterized qualitatively. (Also note that the change of the constraining volume changes the effective pressure,[28] so in principle all peaks in $C_V(T)$ are affected by R_c, but to a much smaller extent.)

The existence of the two structural transformations constitute generic properties of the LJ clusters. In order to characterize these transitions, in Figs. 9 and 11 we show the heat capacities and Q_6 order parameter distributions for several typical two- and three-layer clusters. The $\rho(Q_6, T)$ distributions show the existence of three distinct structural types [ico(M), ico(aM) and liq] for clusters with Mackay global minima and two types [ico(aM) and liq] for clusters with anti-Mackay global minima. The rapid changes in the order parameter distributions occur at temperatures where the corresponding heat capacity peaks are situated. We also note that a structural transition in a finite system is correctly described by a coexistence region,[29] where, e.g., the distribution $\rho(Q_6, T)$ has a bimodal character for some narrow but finite temperature range. Very similar results are observed for all two- and three-layer clusters, which we do not show here.

For the three-layer clusters we also present the core distributions (right column of Fig. 11) $\rho(Q_6^{\text{core}}, T)$ and compare them with the corresponding results for LJ_{55}. One striking observation is that for all the presented cases $\rho(Q_6^{\text{core}}, T)$ looks qualitatively the same with a single abrupt change occurring at temperature $T \sim 0.3$ of the highest maximum of the $C_V(T)$ curve. This proves that the 55-atom core remains

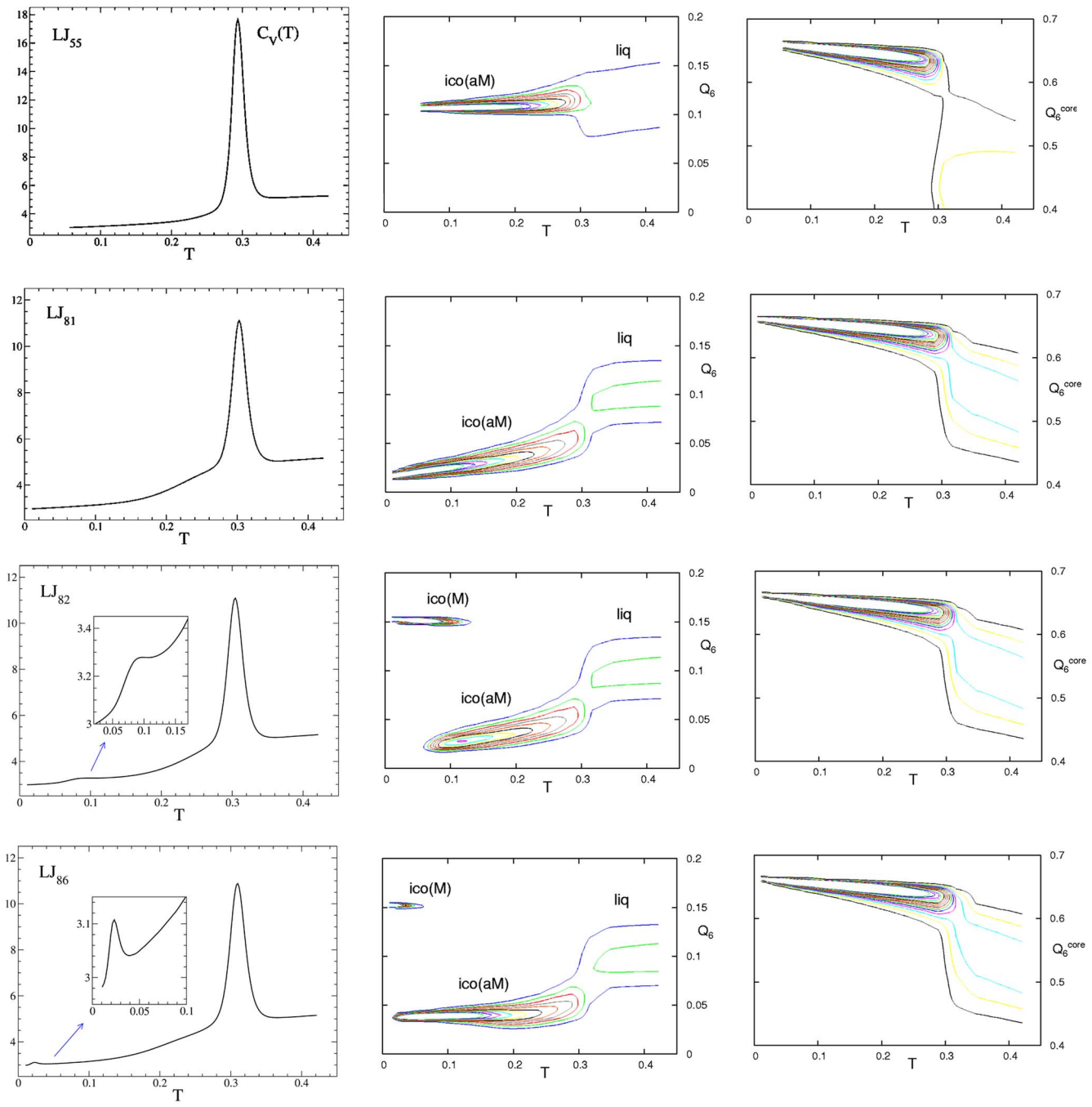

FIG. 11. Left column: Heat capacities of selected three-layer LJ clusters. Middle column: contour plots of the corresponding distributions $\rho(Q_6,T)$ of the orientational bond order parameter Q_6. Right column: the distributions of Q_6^{core} for the 55-atom core of the cluster. The contour levels were somewhat adjusted to best show the distinct features of the distributions, while the same set of contour levels were used for all plots of the same type. The striking similarities in the behavior of $\rho(Q_6^{\text{core}},T)$ proves that the structural transformation occurring at lower temperatures for LJ_n with $n \geqslant 82$ does not involve the core atoms, while the core melting for all clusters occurs at $T \approx 0.3$

stable below this temperature. Unfortunately, a similar structural analysis for the two-layer clusters ($n<55$) is complicated by the fact that the 13-atom core cannot be identified uniquely. In fact, for an anti-Mackay structural motif the local icosahedral coordination is rather typical, thus making the notion of the "core" ambiguous. Therefore, it may be more accurate to characterize the broad high-temperature peak in small clusters as the structural transformation associated with the breaking of the local icosahedral coordination symmetry.

Yet, some clusters display a size-specific behavior, typically occurring at low temperatures. A well-studied example is LJ_{38}, for which the Oh$\rightarrow$ico(M) transition causes a shoulder in the $C_V(T)$ curve at $T\sim 0.12$.[3] For this case the $\rho(Q_6,T)$ distribution expanded to the higher values of Q_6 (Fig. 10 clearly shows the octahedral phase at $T<0.12$, in addition to the generic features present for all the other clusters with Mackay global minima). Another well-studied case corresponds to $n=75-77$ with low-temperature peaks around $T=0.1$ caused by the dec$\rightarrow$ico(aM) transition.[13,22,30] For this

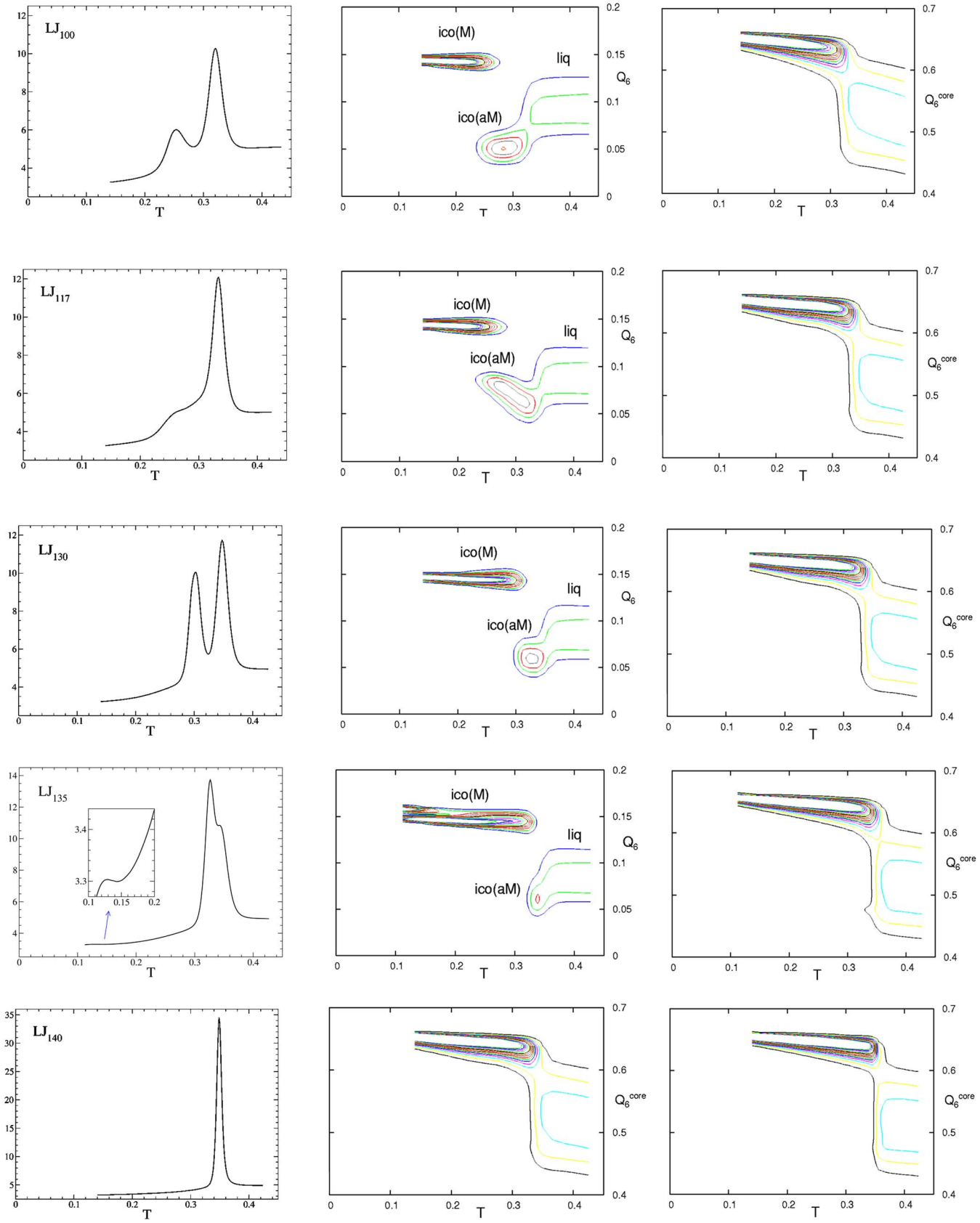

FIG. 11. (*Continued*).

case converged heat capacities and detailed structural analyses based on the use of orientational bond order parameters were presented in Ref. 22. In addition, among all the clusters considered in our calculations caloric curves for $n=21$, 27, 58, and 135 also have small size-specific peaks at low temperatures, possibly due to some rearrangements of the overlayer atoms. Among all these special cases LJ_{135} seems most interesting because its heat capacity curve has, overall, three

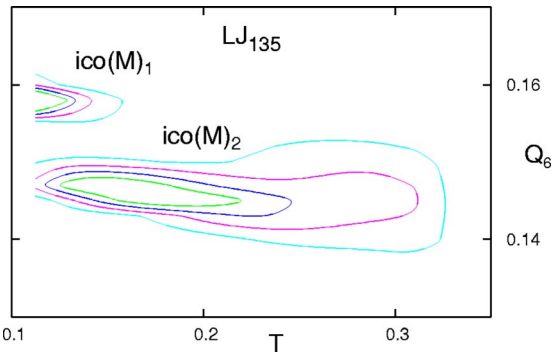

FIG. 12. An expanded region of the $\rho(Q_6,T)$ contour plot for LJ_{135} displaying the bimodal distribution due to the existence of the low-temperature "solid-solid" transition between the two structures shown in Fig. 13

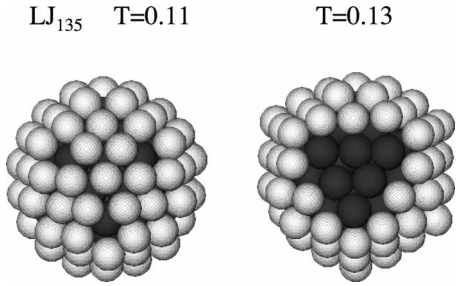

FIG. 13. Snapshot configurations taken from the EMC simulations of LJ_{135} at two different temperatures $T=0.11$ (below the low-temperature peak of the heat capacity) and $T=0.13$ (at the peak maximum). The lower-temperature configuration ($ico(M)_1$ in Fig. 12) corresponds to the global energy minimum, having a perfect icosahedral symmetry. The higher-temperature structure ($ico(M)_2$ in Fig. 12) corresponds to one of the low energy local minima, also highly symmetric and also having a Mackay overlayer.

peaks. The two strong closely spaced peaks around $T \sim 0.34$ correspond to the generic $M \rightarrow aM$ and core-melting transitions. This may be proven by analyzing the order parameter distributions that look similar to the other examples provided in Fig. 11. We were also able to characterize the structural transformation associated with the lowest peak at $T \sim 0.13$. The zoomed $\rho(Q_6,T)$ distribution (Fig. 12) clearly shows the existence of two phases at low temperatures, while $\rho(Q_6^{\text{core}},T)$ does not have any features around $T \sim 0.13$. This proves that this transition is only accompanied by structural transformations within the overlayer. Figure 13 shows two snapshots of different replica configurations from the EMC simulations of LJ_{135} at temperatures $T=0.11$ (i.e., below the peak maximum) and $T=0.13$ (at the peak maximum). The lower-temperature configuration corresponds to the global energy minimum with a perfect icosahedral symmetry. This structure can be obtained from the complete icosahedron, LJ_{147}, by removing atoms from each of its 12 vertices. The higher-temperature structure in Fig. 13 corresponds to one of the low energy local minima, also highly symmetric and also having a Mackay overlayer. This structure can be obtained from LJ_{147} by removing 12 atoms near one of its vertices. The entropy of this configuration is yet greater than that of the global minimum, making it thermodynamically more favorable at $T \sim 0.13$ and leading to a finite peak in $C_V(T)$.

CONCLUSIONS

In this paper we reported results of extensive EMC calculations for LJ clusters for sizes up to $n=147$. We believe that for the temperature ranges considered the main features of the heat capacity curves are reproduced correctly. However, it is still possible that for some clusters, especially with sizes $n \geqslant 89$ the convergence was not sufficient to make a clear judgment on either the shape or the exact location of some peaks in the $C_V(T)$ curves. Only substantially more extensive EMC calculations may clear this issue. However, independent of such possible numerical inaccuracies, our results prove the existence of at least two generic and qualitatively distinct solid-liquid-type transitions in the LJ clusters: a low-temperature $M \rightarrow aM$ transition that occurs within the overlayer and the higher-temperature solid-liquid transition that occurs within the cluster core. Apparently, these interpretations are not easy to justify as just looking at a few (out of 10^{10}) snapshot configurations cannot be sufficient. Our justification in Paper I used the continuity argument, utilizing the analysis of the heat capacity curves as a function of cluster size n. This analysis proved that the presence of the low-temperature peak was directly related to the overlayer symmetry of the global energy minimum. The behavior of the higher-temperature peak as a function of n naturally suggested its relevance to the type of the cluster core (i.e., 13-atom or 55-atom core). In the present work we also performed a more direct analysis of cluster structures utilizing appropriate order parameters, which provided additional evidences for our interpretation.

While these two transitions constitute the generic properties of the LJ clusters in the size range considered, there also is a pronounced size-specific behavior, which manifests itself in the nonmonotonous dependence of the transition temperatures as a function of cluster size, as well as in the existence of special cases ("magic numbers") corresponding to highly symmetric but possibly nonicosahedral global minima. The latter clusters display a size-specific behavior that often results in low-temperature solid-solid-type structural transformations.

Our results are a manifestation of the complexity of the properties of finite systems (clusters) which is expected to disappear only in the bulk limit when the surface effects become relatively unimportant for equilibrium properties. LJ clusters with hundreds and even thousands of atoms are still far from the bulk limit and as such are expected to display a similar or perhaps an even more complex behavior. When this paper was submitted for publication we learned about the recent study by Noya and Doye[31] on LJ_{309}, whose global minimum is the complete four-layer Mackay icosahedron. Unlike the smaller magic number clusters ($n=13$, 55, and 147), LJ_{309} has two sharp peaks in the $C_V(T)$ curve, with the lower-temperature peak corresponding to a complex surface reconstruction transition, possibly involving several competing processes. Therefore, it is likely that the intermediate-size clusters with $147 < n < 309$ may undergo more than two generic structural transformations.

The extraordinary complexity of LJ clusters presents a great challenge for accurate numerical simulations, even without accounting for quantum effects. Yet another interest-

ing question emerging from the present and previous studies is how the quantum effects, due to the finite mass of the rare gas atoms, change their phase diagram. As an example, Ref. 32 explores the effect of quantum delocalization on the melting of LJ clusters as a function of the de Boer parameter. Recently, several steps toward answering this and related questions, along with the development of the numerical techniques to perform the corresponding quantum statistical mechanics calculations, were particularly made in Refs. 24 and 33–35. For example, Refs. 24 and 35 show that none of the nonicosahedral structures observed for some classical two- and three-layer LJ clusters are energetically stable for the corresponding neon clusters. Moreover, the quantum nature of neon clusters favors the anti-Mackay more than the Mackay symmetry and as such has a substantial effect on the critical parameters of the Mackay-anti-Mackay transition.[35]

Unfortunately, an experimental confirmation of our findings appears currently impossible due to the known technical challenges associated with measurements on neutral rare gas clusters. We note, though, that indications of surface melting effects have been observed in recent experiments on ionized aluminum clusters.[36]

ACKNOWLEDGMENTS

The NSF support (Grant No. CHE-0414110) is acknowledged. One of the authors (V.A.M.) is an Alfred P. Sloan research fellow. We are grateful to Florent Calvo for his numerous comments and, particularly, for the suggestion to consider the distributions of the orientational bond order parameters. Figures 1 and 13 were generated with the VMD software package.[37]

[1] D. J. Wales, M. A. Miller, and T. R. Walsh, Nature (London) **394**, 758 (1998).
[2] J. P. K. Doye and F. Calvo, J. Chem. Phys. **116**, 8307 (2002).
[3] J. P. Neirotti, F. Calvo, D. L. Freeman, and J. D. Doll, J. Chem. Phys. **112**, 10340 (2000).
[4] F. Calvo, J. P. Neirotti, D. L. Freeman, and J. D. Doll, J. Chem. Phys. **112**, 10350 (2000).
[5] J. P. K. Doye, M. A. Miller, and D. J. Wales, J. Chem. Phys. **110**, 6896 (1999).
[6] C. J. Geyer, in *Computing Science and Statistics: Proceedings of the 23rd Symposium on the Interface*, edited by E. K. Keramidas (Interface Foundation, Fairfax Station, 1991), p. 156.
[7] K. Hukushima and K. Nemoto, J. Phys. Soc. Jpn. **65**, 1604 (1996).
[8] D. D. Frantz, J. Chem. Phys. **115**, 6136 (2001).
[9] P. A. Frantsuzov and V. A. Mandelshtam, Phys. Rev. E **72**, 037102 (2005).
[10] J. A. Northby, J. Chem. Phys. **87**, 6166 (1987).
[11] J. P. K. Doye, D. J. Wales, and R. S. Berry, J. Chem. Phys. **103**, 4234 (1995).
[12] R. H. Leary, J. Global Optim. **11**, 35 (1997).
[13] D. J. Wales and J. P. K. Doye, J. Phys. Chem. A **101**, 5111 (1997).
[14] F. Calvo and J. P. K. Doye, Phys. Rev. E **63**, 010902(R) (2001).
[15] H.-P. Cheng and R. S. Berry, Phys. Rev. A **45**, 7969 (1992).
[16] F. Calvo and P. Labastie, Chem. Phys. Lett. **258**, 233 (1996).
[17] J. P. K. Doye and D. J. Wales, Z. Phys. D: At., Mol. Clusters **40**, 466 (1997).
[18] S. C. Hendy and B. D. Hall, Phys. Rev. B **64**, 085425 (2001).
[19] F. Calvo and F. Spiegelman, J. Chem. Phys. **120**, 9684 (2004).
[20] P. J. Steinhardt, D. R. Nelson, and M. Ronchetti, Phys. Rev. B **28**, 784 (1983).
[21] R. M. Lynden-Bell and D. J. Wales, J. Chem. Phys. **101**, 1460 (1994); J. P. K. Doye and D. J. Wales, *ibid.* **102**, 9673 (1995); C. Chakravarty, Mol. Phys. **100**, 3777 (2002).
[22] V. A. Mandelshtam, P. A. Frantsuzov, and F. Calvo, J. Phys. Chem. A **110**, 5326 (2006).
[23] C. Predescu, M. Predescu, and C. V. Ciobanu, J. Chem. Phys. **120**, 4119 (2004).
[24] C. Predescu, P. A. Frantsuzov, and V. A. Mandelshtam, J. Chem. Phys. **122**, 154305 (2005).
[25] H. B. Liu and K. D. Jordan, J. Phys. Chem. A **109**, 5203 (2005).
[26] http://www-wales.ch.cam.ac.uk/CCD.html
[27] A. M. Ferrenberg and R. H. Swendsen, Phys. Rev. Lett. **61**, 2635 (1988).
[28] D. Sabo, D. L. Freeman, and J. D. Doll, J. Chem. Phys. **122**, 094716 (2005).
[29] H. L. Davis, J. Jellinek, and R. S. Berry, J. Chem. Phys. **86**, 6456 (1986); T. L. Beck, J. Jellinek, and R. S. Berry, *ibid.* **87**, 545 (1987); D. J. Wales and J. P. K. Doye, *ibid.* **103**, 3061 (1995).
[30] J. P. K. Doye and F. Calvo, J. Chem. Phys. **116**, 8307 (2002).
[31] E. G. Noya and J. P. K. Doye, J. Chem. Phys. **124**, 104503 (2006).
[32] C. Chakravarty, J. Chem. Phys. **103**, 10663 (1995).
[33] F. Calvo, J. P. K. Doye, and D. J. Wales, J. Chem. Phys. **114**, 7312 (2001).
[34] C. Predescu, D. Sabo, J. D. Doll, and D. L. Freeman, J. Chem. Phys. **119**, 12119 (2003); D. Sabo, C. Predescu, J. D. Doll, and D. L. Freeman, *ibid.* **121**, 856 (2004).
[35] P. A. Frantsuzov, D. Meluzzi, and V. A. Mandelshtam, Phys. Rev. Lett. **96**, 113401 (2006).
[36] G. A. Breaux, C. M. Neal, B. Cao, and M. F. Jarrold, Phys. Rev. Lett. **94**, 173401 (2005).
[37] W. Humphrey, A. Dalke, and K. Schulten, J. Mol. Graphics **14**, 33 (1996).